RSC Advances

ROYAL SOCIETY OF CHEMISTRY

www.rsc.org/advances

Maleimide: A Potential Building Block for the Design of Proton Exchange Membranes Studied by *Ab Initio* Molecular Dynamics Simulations

Xuejiao Li, Liuming Yan*, Baohua Yue

Department of Chemistry, College of Sciences, Shanghai University, 99 Shangda Road, Shanghai 20044, China

ABSTRACT

Ab initio molecular dynamics (AIMD) simulations are applied to the study of proton transport in solid state maleimide. The AIMD simulations reproduce correctly the structural and energetic characteristics. The simulations reveal the direct proton hopping between two maleimide molecules, and the proton hopping frequency is evaluated. The temperature dependence of proton hopping frequency obeys the Arrhenius activation process with an activation energy of 4.39 kcal·mol^{-1}. Finally, it is proposed that maleimide is potential building block for the design of high-temperature proton exchange membranes.

Keywords: proton exchange membrane fuel cell; proton exchange membrane; maleimide; proton transport; *ab initio* molecular dynamics simulation

1. Introduction

During the past decades, proton exchange membrane fuel cells (PEMFCs) have received tremendous attention as novel energy conversion devices because of their environmental friendliness and high fuel utilization efficiency. High-temperature proton exchange membrane fuel cells (HT-PEMFCs) are particularly desirable due to their outstanding advantages, such as humidity-independent performances, enhanced electrocatalytic activity, and improved tolerance

* Corresponding author. Tel.: 8621-66132405, fax: 8621-66132405. E-mail: liuming.yan@shu.edu.cn

to impurities in fed-gas.[1] Nevertheless, the large scale commercialization of HT-PEMFCs depends largely on the high-temperature performances of the proton exchange membranes (PEMs), or the high-temperature proton exchange membranes (HT-PEMs).[2-5]

The development of PEMFCs depends heavily on the success of perfluorosulfonic acid polymers (PFSA), such as NAFION, owing to their high proton conductivity, excellent chemical and electrochemical stability. However, the application of PFSA in PEMFCs is limited to temperatures that liquid water exists in the membrane. At high temperature, the water which hydrates PFSA evaporates and the proton conductivity of PFSA degrades.[6-7] Therefore, the development of novel proton conducting materials possessing high proton conductivity at high temperature is of essential importance for the development of HT-PEMFCs.

The high-temperature proton conductivity of PFSA can be improved by doping with SiO_2, TiO_2, ZrO_2, $Zr(HPO_4)_2$, etc. as water adsorption or retention materials,[8-12] or by addition of H_3PO_4, imidazole, triazole, benzimidazole, pyrazole, etc. to substitute water as hydration solvent.[13-22] The other option for HT-PEMs is to develop new proton conducting materials with proton conductivity independent upon hydration. For example, polymeric phosphonic acid possesses much better proton conductivity under dehydrated or even anhydrous states attributing to the self-dissociation of phosphonic acid at high temperature.[23] Recently, we observed the synergetic proton transport effect, the orders of magnitude increase in proton conductivity, in acid-base polymeric composites and acid-base amphoteric polymers consisting of phosphonic acid groups and triazolyl groups.[17-19]

Maleimide (MI) is an interesting molecule showing amphoteric characteristics, its imide proton (>N−H) shows weak acidity with a dissociation constant pK_a at 5.57 in aqueous solution evaluated from our conductivity measurement, and two acyl oxygen atoms show strong affinity

for protons from imide nitrogen atoms. Therefore, complex hydrogen bonding (H-bonding) network forms in solid state MI. As a matter of fact, the structure of a MI molecule, in terms of H-bonding donor and acceptor, is similar to a 1*H*-1,2,3-triazole molecule, which is widely accepted as building block in the design of proton conducting materials, especially the proton conducting materials at high temperature under a water deficient environment.[24-26] As being shown in triazole, the tautomerization is an important characteristic for the proton transfer in hydrophilic compounds. MI also shows abundant tautomerization pathways, especially with the mediation of other hydrophilic compounds. In this aspect, Kalia *et al.* studied both the gas phase and water-assisted tautomerization of MI using density functional theory (DFT) calculations.[27] Based on these considerations, we measured the overall conductivity of MI, and observed an unexpected high conductivity of 6.46 $mS \cdot cm^{-1}$ at 60 °C and 90% RH (relative humidity). This conductivity is even higher than that of NAFION at about 6 $mS \cdot cm^{-1}$ at 40% RH.[28] Therefore, we propose that MI can be used as potential building block for the design of high-temperature proton conducting materials.

Molecular dynamics (MD) simulations, especially *ab initio* molecular dynamics (AIMD) simulations, are widely applied to the study of proton transport in the field of proton exchange membrane. For example, Vilčiauskas and Tuckerman *et al.* investigated the proton transport in phosphoric acid and the proton dynamics in a system composed of phosphoric acid and imidazole using AIMD simulation, and attributed the reduced proton density in *N*-heterocycles doped H_3PO_4 to the strong proton affinity of imidazole.[29-30] Iannuzzi *et al.* presented the atomistic details of the fast rearrangement of H-bonding which sustains the proton transfer in imidazole-based heterocyclic molecular crystals and resolved all the resonant peaks in experimental spectra using AIMD simulations.[31-32] Ludueña *et al.* proposed a carrier-mediated

Grotthuss mechanism of proton conducting and depicted an atomistic picture for the long-distance proton transport using a steered AIMD approach.[33] Hayes *et al.* studied the proton transport in triflic acid pentahydrate using *ab initio* path integral molecular dynamics.[34] Yan *et al.* studied the proton transfer in acidified aqueous solution of methanol, and observed the direct proton transfer using AIMD simulations.[35]

In this work, AIMD simulations are applied to the characterization of proton transport in solid state MI. The molecular structure, frequency spectra, velocity autocorrelation functions, and proton hopping frequency are evaluated. These characteristics can provide essential understanding of the MI as building block for the design of proton conducting polymers.

2. Calculation methods

The Car-Parrinello molecular dynamics simulation (CPMD) is an important theoretical method for the investigation of dynamic properties of molecular systems including transport and chemical reactions. In this research, the proton transport in solid state MI is studied by use of the CPMD package.[36] The simulated system consists of 8 MI molecules and one unbounded proton with triclinic crystal symmetry and P-1 space group as shown in **figure 1**. The unbounded proton is labeled as H1 and placed between two MI molecules, the distances between H1 and two closest oxygen atoms O39 and O48 are 1.521 and 2.282 Å, respectively, in the initial configuration. And the atomic coordinates of the initial configuration are supplied as supplementary information in **table S1**. In our CPMD simulation, we follow the widely practiced method by addition of an unbound proton to the simulated system to ease the observation of proton transport, and the overall charge of the system is +1.0.[37-39] The cell parameters are adapted from experimental parameters of X-ray diffraction at 150 K: a = 6.768 Å,

b = 10.675 Å, c = 12.384 Å, and α = 81.37°, β = 77.01°, γ = 74.77°, and the cell volume is 837.258 Å^3 and overall density is 1.556 g cm^{-3}.[40] Considering the great computational cost of CPMD simulations, the simulated systems are usually much smaller than those of the classic MD simulations. On the other hand, a simulation with only one unit cell is sufficient to reproduce the characteristic of proton transport despite of the fact that statistical errors may be significant for quantitative values.[41-44]

The generalized gradient approximation (GGA) functionals and hybrid functionals are widely accepted in quantum chemistry calculations because these functionals can provide reasonably accurate predictions for geometries and thermodynamics of small covalent molecules.[45-47] In our CPMD simulations, the hybrid BLYP exchange correlation functionals are used to approximate the energy of valent electrons,[48] which can provide an adequate description of crystalline systems with H-bonding,[31-32, 49] the Troullier-Martins (MT) norm-conserving pseudo-potentials are used to represent the core electrons,[50] and the plane wave basis set is used to expand the Kohn-Sham wave functions with a cutoff energy at 85 rydberg. These pseudopotentials are provided in the CPMD extended library package, and cutoff energies of plane wave basis set at 25, 30, 40 and 70 rydberg for H, C, N, and O are recommended to reproduce meaningful results.[51-53] The cutoff energy used in this study is significantly larger than the maximum cutoff energy recommended, thus better simulations results can be expected.

During our CPMD simulation, the initial wave functions are optimized using the direct inversion method with a convergence criterion of 1.0x10^{-7} a.u.. After the optimization of initial wave functions, about 9 ps of CPMD simulation is carried out to relax the simulation cell into equilibrium configuration at target temperature in NVT ensemble using the velocity rescaling algorithm. And then, production simulation is carried out in NVT ensemble using a

Nosé-Hoover chain thermostat with ion thermostat frequency at 3500 cm^{-1}, electron thermostat frequency at 15000 cm^{-1}. Throughout these CPMD simulations, a fictitious electron mass of 500.0 a.u. and a time step of 4.0 a.u. are used.

3. Results and discussion

3.1 Energetics for solid state MI

The CMPD simulation is carried out in NVT ensemble at 363.15 K, and the real ionic temperature fluctuates along an average temperature of 362.57 K with a standard deviation of 31.49 K. The evolutions of the kinetic and potential energies during CPMD simulation are shown in **figure 2**. The total energy E_{tot} fluctuates along an average value of -531.28119 a.u. with a tiny standard deviation of 8.4748×10^{-4} a.u.. The Kohn-Sham energy, E_{KS}, which represents the summation of potential energy of the electrons, electrostatic attraction energy between electrons and ionic cores, and electrostatic repulsion between ionic cores, fluctuates with a large standard deviation at about 0.01343 a.u.. Compared with the total energy, the greater fluctuation of Kohn-Sham energy compensates the fluctuation of kinetic energy of ionic cores, as the Kohn-Sham energy and kinetic energy of ionic cores constitutes the classic energy which fluctuates with a much smaller standard deviation. The total kinetic energy of ionic cores fluctuates along 0.12598 a.u. with a standard deviation of 0.01315 a.u.. In addition, the fictitious kinetic energy, which is related to the evolution of wave functions in a manner of particles, fluctuates along 0.02002 a.u. with a standard deviation of 9.3556×10^{-4} a.u..

3.2 Radial distribution functions

Figure 3 shows the radial distribution functions for the N−O, N−H, and O−H atomic pairs simulated in NVT ensemble at 363.15 K, where H represents the acidic protons (including the

unbounded proton). For the N−H atomic pair, a high and sharp peak at 1.020 Å represents the N−H bond, and is in good agreement with the bond distance of 1.022 Å evaluated from DFT calculations at ωB97X-D/6-311+G(2d,p) level of theory. For the O−H atomic pair, the first peak at 1.005 Å, relatively low, clearly shows that the acidic proton is attracted by the O atom. The broad peak at 1.845 Å is attributed to the intermolecular H-bonding of N–H···O, and the third peak at 2.685 Å represents the O−H distance between the acyl oxygen atom and the acidic proton in the same MI molecule in good agreement with XRD observation at 2.681 Å.[40] For the N−O atomic pair, a sharp peak at 2.325 Å corresponds to the intramolecular N−O distance, and the second peak at 2.895 Å to the intermolecular H-bonding N−H···O. This intermolecular H-bonding N−H···O is in good agreement with experimental values between 2.851 and 2.917 Å.[40]

3.3 Frequency analysis in solid state MI

Frequency analysis can provide vital information to the understanding of the optical and mechanical responses of condensed molecular systems.[40, 54] In addition, bond stretching vibrational spectra are essential criteria for the validation of simulation results. **Figure 4a** summarizes the bond stretching vibrational spectra evaluated via fast Fourier transformation (FFT) of the time dependences of interatomic distances recorded during CPMD simulations in NVT ensemble at 363.15 K. These bond stretching vibrational spectra are consistent with experimental FTIR spectrum as shown in **figure 4b**. Since the CPMD simulations usually underestimate the stretching frequency attributing to electrostatic and crystal field effects, the CPMD simulated frequencies in **figure 4a** are scaled by factors of 1.0376.[43, 55] For the spectrum of C−H bond, the major peak at 3152 cm^{-1} is consistent with the corresponding FTIR peak at about 3100 cm^{-1}. For the N−H spectrum, the major peak at 3264 cm^{-1} is much broader

than the C−H peak revealing the strong intermolecular H-bonding interaction between N−H and the acyl oxygen atom. The peak for the O−H spectrum at 3223 cm^{-1} is lower than that of N−H spectrum and is consistent with experimental observation.[56] From these discussions, it can be concluded that our CPMD simulations give reasonable vibrational characteristics compared with experimental FTIR spectrum.

3.4 Velocity autocorrelation functions

The atomic velocity autocorrelation functions (VACFs) are evaluated as,

$$\mathrm{VACF_A}(\tau) = \frac{1}{N_\mathrm{A}(m-\tau)} \sum_{\tau_0=1}^{m-\tau} \sum_{i=1}^{N_\mathrm{A}} \mathbf{v}_i(\tau_0) \cdot \mathbf{v}_i(\tau_0+\tau) \qquad (1)$$

where subscript A represents the atom types, N_A is the number of atoms for atom type A, $\mathbf{v}_i$ is velocity for atom i, τ_0 is the initial time, and τ is the time elapsed after the initial time. The VACFs for the acidic hydrogen atoms (H_a), the non-acidic hydrogen atoms (H_n), the nitrogen atoms (N), and the oxygen atoms (O) are shown in **figure 5a**. It can be seen that the initial decays of the VACFs for H_a and H_n are much faster than those for N and O indicating the strong short time dynamic correlation between the protons and their environment. However, all the VACFs fluctuate rapidly with large amplitudes because the simulated system is small and simulation time is short, and thus statistics errors are large.[35]

The corresponding spectra of VACFs are shown in **figure 5b**. For both the acidic and non-acidic protons, the strong peaks at about 3046 cm^{-1} are correspondent with the stretching vibration of N–H and C–H bonds. While the acidic proton possesses a slightly lower frequency compared with the non-acidic protons for about 42 cm^{-1}, in consistent with the fact that an acidic proton is more loosely bounded thus slower velocity exchange with its environment.

3.5 Proton hopping between MI molecules

The direct observation of the hopping of the unbounded proton (H1) between two oxygen

atoms (O39 and O48) in two adjacent MI molecules is depicted in **figure 6**. **Figure 6a** shows the probability distributions of the interatomic distances of O39–O48, H1–O39 and H1–O48 evaluated from CPMD simulation in NVT ensemble at 363.15 K. The O39–O48 distance fluctuates between 2.364 to 3.228 Å, with a most probability at 2.748 Å; the H1–O39 distance fluctuates between 0.919 to 1.164 Å with a most probability at 1.004 Å; and the H1–O48 fluctuates between 1.276 to 2.328 Å with a most probability at 1.624 Å. These characteristics are consistent with the corresponding radial distribution functions.

From the overall probability distributions of interatomic distance H1–O39 at given O39–O48 distance (**figures 6b and 6c**), it can been seen that the most probable H1–O39 distance slightly decreases from 1.119 to 0.919 Å, as the O39-O48 distance increases from 2.385 to 3.228 Å. On the other hand, the most probable H1–O48 distance fluctuates in a much greater scope ranging from 1.292 to 2.258 Å, at the same O39–O48 distance range. Moreover, the H1–O39 distance and H1–O48 distance intersect at about 1.221 Å given the O39–O48 distance at about 2.390 Å. From these observations, it could be concluded that the proton H1 hops between O39 and O48 as the O39–O48 distance decreases to about 2.390 Å.

Proton conducting corresponds to the macroscopic proton transport or the long distance proton transport, and can be divided into a series of microscopic steps of atomic movement. If the H-bonding network is the essential structural requirement for the macroscopic proton transport, the proton hopping and conformational rearrangement are two essential dynamic steps in the process of macroscopic proton transport.[57] For example, in the so-called "hop-turn" mechanism, the effective proton transport includes the proton hopping and the bond rotation or the reorientation of the proton acceptors.[58-60] Our CPMD simulations clearly show that the protons hop between two oxygen atoms in solid state MI, and thus fulfill one of the two essential

microscopic steps in the macroscopic proton transport. Compared with the proton hopping, the reorientation of the proton acceptors, corresponding to the rotational movement of the MI molecule in this context, is much slower, and the CPMD simulation of the rotational movement of the MI molecule is infeasible attributing to the limited simulation time and size of simulated system.

Furthermore, our CPMD simulations show that the H–O bond breaking and building occur simultaneously at the crossover point where the interatomic distances of H1–O39 and H1–O48 possess the same value of 1.221 Å as shown in **figures 6b** and **6c**. The simultaneous H–O bond breaking and building requires the minimum free energy compared with the H–O bond breaking followed by H–O bond rebuilding. In order to evaluate directly the energetics of proton hopping, the potential energy surfaces along the reaction coordinate that define the proton exchange between two MI molecules in an isolated system consisting of only two MI molecules and an unbounded proton are evaluated using DFT calculation at theory level of ωB97X-D/6-311+G(2d,p) as shown in **figure 6d**. From **figures 6d**, it can be seen that the potential energy surfaces depend on the relative position of the two MI molecules or the distance between two oxygen atoms $d_{O–O}$, and the approaching of the two MI molecules results the decreasing of potential barrier for proton hopping. The highest potential barrier is about 1.93 kcal·mol^{-1}, and the potential barrier disappears at crossover position ($d_{O–O}$ = 2.34 Å). At crossover position, the proton hopping occurs between the two oxygen atoms without any barrier. The potential energy along the reaction coordinate used to define the H1 exchange between O39 and O48 can also be evaluated as potential of mean force from an umbrella sampling or other bias-based sampling simulation, or from the proton vibrational eigenfunctions and eigenvalues incorporating statistical sampling, nuclear quantum effects, and effects of the environment.[41, 61]

However, the energetics of proton hopping is more complex than a static potential energy surface or a potential of mean force along the reaction coordinate. As a matter of fact, the thermodynamic motion of the surrounding atoms provides the driving force for proton hopping, and both results represent part of the basic physics despite of their quantitative difference.

The proton hopping frequency f_{hop} is evaluated as the times of hopping per second for each unbounded proton by counting the total times of hopping of H1 between O39 and O48,

$$f_{\text{hop}} = \frac{N_{\text{cross}}}{N_{\text{p}}\Delta t} \tag{2}$$

where N_{cross} is the total times of hopping observed in a time period of Δt in a simulation cell consisting of N_{p} unbounded acidic protons. From our CPMD simulation, it is evaluated that the proton hopping frequency is about $1.034\text{x}10^{11}$ s^{-1} for each unbounded acidic proton at 363.15 K, in the same range as the proton hopping rate in hydrogen bonded chains at about $\sim 10^{11}$ s^{-1}.[62-64] As the simulation temperature increases, the proton hopping frequency increases. From **figure 7**, which shows the temperature dependence of proton hopping frequency, it can be concluded that the proton hopping obeys an Arrhenius activation process. And the phenomenological activation energy for proton hopping is evaluated at 4.39 $\text{kcal}\cdot\text{mol}^{-1}$, revealing the ease of hopping of an unbounded proton in MI system.

Bounded protons are not transportable, and ionization is the first step of the proton transport. The proton conductivity is proportion to the product of the proton hopping frequency, concentration of unbounded protons, and the rotational movement of the MI molecule. Since the pK_a of MI in aqueous solution is 5.57 and overall concentration of solid state MI is at 16.20 $\text{mol}\cdot\text{dm}^{-3}$, a rough approximation for the concentration of unbounded or ionized protons is evaluated at $6.6\text{x}10^{-3}$ $\text{mol}\cdot\text{dm}^{-3}$, equivalent to an ionization degree of $4.08\text{x}10^{-4}$. It should emphasize that this is a very rough approximation since the pK_a of MI in aqueous solution is

used. If a hopping efficiency is defined to describe the contribution of rotational movement of the MI molecules to macroscopic proton transport, the hopping efficiency is dependent on the structure of the solid state MI and thus its morphology. The energy barrier for proton transport evaluated from DFT calculations at theory level of ωB97X-D/6-311+G(2d,p) is about 1.93 kcal·mol^{-1}, which agrees with the experimentally determined activation energy for proton oscillatory shuttling.[65] Considering the potential energy surface from DFT calculations only represents a rough approximation to the solid state CPMD simulation, this energy barrier is consistent with the phenomenological activation energy for proton hopping of the unbounded protons at 4.39 kcal·mol^{-1}.

4. Conclusions

AIMD simulations are carried out to directly investigate the proton hopping characteristics in solid state MI. The energetics, structural characteristics in terms of radial distribution functions, bond stretching vibrational frequency spectra, velocity autocorrelation functions, and proton hopping characteristics are evaluated. Compared with experimental observations, the CPMD simulations give reasonable structure and frequency spectra.

The simulations reveal that the H–O and H···O distances in the O–H···O H-bonding fluctuate depending on the overall distance between the two oxygen atoms. At large O···O distance, the potential surface possesses a two-well structure along the proton transport coordinate, and the equilibrium position of the proton closes to one of the oxygen atoms at a most probability distance of 1.004 Å. As the two oxygen atoms approaches, the potential barrier gradually decreases and the equilibrium position of the proton approaches to the center of the two oxygen atoms. At crossover position, the potential barrier disappears, and the proton

hopping occurs between the two oxygen atoms. The proton hopping frequency between two MI molecules is about 1.034×10^{11} s^{-1} for each unbounded acidic proton at 363.15 K, and increases exponentially with the reciprocal of temperature. A phenomenological activation energy at about 4.39 $kcal \cdot mol^{-1}$ is evaluated by application of the Arrhenius activation process.

In conclusion, MI possesses both H-bonding donor and acceptor, and forms complex H-bonding network. The protons can hop easily between MI molecules, and MI can perform both as proton transport media and solvation agent. Therefore, we proposed that MI could be used as potential building block for the design of PEMs for HT-PEMFCs.

Acknowledgements

The authors thank the financial support from the Chinese National Science Foundation (Nos. 21376147, 21573143), the Innovation Program of Shanghai Municipal Education Commission (13ZZ078), and the 085 Knowledge Innovation Program, and they also acknowledge the High Performance Computing Center and Laboratory for Microstructures, Shanghai University, for computing and structural characterization support.

References

1. Li, Q.; He, R.; Jensen, J. O.; Bjerrum, N. J. PBI-based polymer membranes for high temperature fuel cells-preparation, characterization and fuel cell demonstration. *Fuel Cells* **2004**, *4*(3), 147-159.
2. Zhang, H.; Shen, P. K. Recent development of polymer electrolyte membranes for fuel cells. *Chem. Rev.* **2012**, *112*(5), 2780-2832.
3. Bose, S.; Kuila, T.; Nguyen, T. X. H.; Kim, N. H.; Lau, K.; Lee, J. H. Polymer membranes

for high temperature proton exchange membrane fuel cell: Recent advances and challenges. *Prog. Polym. Sci.* **2011**, *36*(6), 813-843.

4. Peighambardoust, S.; Rowshanzamir, S.; Amjadi, M. Review of the proton exchange membranes for fuel cell applications. *Int. J. Hydrogen Energy* **2010**, *35*(17), 9349-9384.
5. Kreuer, K. On the development of proton conducting polymer membranes for hydrogen and methanol fuel cells. *J. Membr. Sci.* **2001**, *185*(1), 29-39.
6. Doyle, M.; Choi, S. K.; Proulx, G. High-temperature proton conducting membranes based on perfluorinated ionomer membrane-ionic liquid composites. *J. Electrochem. Soc.* **2000**, *147*(1), 34-37.
7. Carbone, A.; Pedicini, R.; Sacca, A.; Gatto, I.; Passalacqua, E. Composite SPEEK membranes for medium temperature polymer electrolyte fuel cells. *J. Power Sources* **2008**, *178*(2), 661-666.
8. Dresch, M. A.; Matos, B. R.; Fonseca, F. C.; Santiago, E. I.; Carmo, M.; Lanfredi, A. J. C.; Balog, S. Small-angle X-ray and neutron scattering study of Nafion-SiO_2 hybrid membranes prepared in different solvent media. *J. Power Sources* **2015**, *274*, 560-567.
9. Jiang, S. P. Functionalized mesoporous structured inorganic materials as high temperature proton exchange membranes for fuel cells. *J. Mater. Chem. A* **2014**, *2*(21), 7637-7655.
10. Mishra, P. S.; Solanki, J. N.; Murthy, Z. V. P. TiO_2 nanoparticles synthesis for application in proton exchange membranes. *Cryst. Res. Technol.* **2013**, *48*(11), 969-976.
11. Alberti, G.; Casciola, M.; D'Alessandro, E.; Pica, M. Preparation and proton conductivity of composite ionomeric membranes obtained from gels of amorphous zirconium phosphate

sulfophenylenphosphonates in organic solvents. *J. Mater. Chem.* **2004**, *14*(12), 1910-1914.

12. Shao, Z.-G.; Xu, H.; Li, M.; Hsing, I.-M. Hybrid Nafion–inorganic oxides membrane doped with heteropolyacids for high temperature operation of proton exchange membrane fuel cell. *Solid State Ionics* **2006**, *177*(7), 779-785.
13. Mangiatordi, G. F.; Hermet, J.; Adamo, C. Modeling proton transfer in imidazole-like dimers: A density functional theory study. *J. Phys. Chem. A* **2011**, *115*(12), 2627-2634.
14. Subbaraman, R.; Ghassemi, H.; Zawodzinski, T. Triazole and triazole derivatives as proton transport facilitators in polymer electrolyte membrane fuel cells. *Solid State Ionics* **2009**, *180*(20), 1143-1150.
15. Martwiset, S.; Yavuzcetin, O.; Thorn, M.; Versek, C.; Tuominen, M.; Coughlin, E. B. Proton conducting polymers containing 1*H*-1,2,3-triazole moieties. *J. Polym. Sci. A Polym. Chem.* **2009**, *47*(1), 188-196.
16. Çelik, S. Ü.; Akbey, Ü.; Graf, R.; Bozkurt, A.; Spiess, H. W. Anhydrous proton-conducting properties of triazole-phosphonic acid copolymers: a combined study with MAS NMR. *Phys. Chem. Chem. Phys.* **2008**, *10*(39), 6058-6066.
17. Zhang, Y. P.; Yue, B. H.; Han, S. Y.; Yan, L. M. Synergetic proton conducting effect in acid-base composite of phosphonic acid functionalized polystyrene and triazolyl functionalized polystyrene. *RSC Adv.* **2014**, *4*(64), 33702-33712.
18. Yue, B. H.; Yan, L. M.; Han, S. Y.; Xie, L. Q. Proton transport pathways in an acid-base complex consisting of a phosphonic acid group and a 1,2,3-triazolyl group. *J. Phys. Chem. B* **2013**, *117*(26), 7941-7949.

19. Xie, L. Q.; Liu, H. T.; Han, S. Y.; Yue, B. H.; Yan, L. M. Hydrogen bond and proton transport in acid-base complexes and amphoteric molecules by density functional theory calculations and ^{1}H and ^{31}P nuclear magnetic resonance spectroscopy. *J. Phys. Chem. B* **2013**, *117*(50), 16345-16355.

20. Di, S. Q.; Yan, L. M.; Han, S. Y.; Yue, B. H.; Feng, Q. X.; Xie, L. Q.; Chen, J.; Zhang, D. F.; Sun, C. Enhancing the high-temperature proton conductivity of phosphoric acid doped poly(2,5-benzimidazole) by preblending boron phosphate nanoparticles to the raw materials. *J. Power Sources* **2012**, *211*, 161-168.

21. Zhang, D. F.; Yan, L. M. Probing the acid-base equilibrium in acid-benzimidazole complexes by ^{1}H NMR spectra and density functional theory calculations. *J. Phys. Chem. B* **2010**, *114*(38), 12234-12241.

22. Yan, L.; Zhu, S.; Ji, X.; Lu, W. Proton hopping in phosphoric acid solvated NAFION membrane: a molecular simulation study. *J. Phys. Chem. B* **2007**, *111*(23), 6357-6363.

23. Lee, S. I.; Yoon, K. H.; Song, M.; Peng, H.; Page, K. A.; Soles, C. L.; Yoon, D. Y. Structure and properties of polymer electrolyte membranes containing phosphonic acids for anhydrous fuel cells. *Chem. Mater.* **2011**, *24*(1), 115-122.

24. Zhou, Z.; Liu, R.; Wang, J. H.; Li, S. W.; Liu, M. L.; Bredas, J. L. Intra- and intermolecular proton transfer in 1*H*(2*H*)-1,2,3-triazole based systems. *J. Phys. Chem. A* **2006**, *110*(7), 2322-2324.

25. Li, S. W.; Zhou, Z.; Zhang, Y. L.; Liu, M. L.; Li, W. 1*H*-1,2,4-triazole: An effective solvent for proton-conducting electrolytes. *Chem. Mater.* **2005**, *17*(24), 5884-5886.

26. Zhou, Z.; Li, S. W.; Zhang, Y. L.; Liu, M. L.; Li, W. Promotion of proton conduction in polymer electrolyte membranes by 1*H*-1,2,3-triazole. *J. Am. Chem. Soc.* **2005**, *127*(31), 10824-10825.

27. Kalia, S.; Sharma, A.; Kaith, B. S. *Ab initio* study of gas phase and water-assisted tautomerization of maleimide and formamide. *J. Chem. Sci.* **2007**, *119*(6), 617-624.

28. Sone, Y.; Ariyama, Y.; Uno, M.; Naito, H.; Ino, H. Proton conductivity of the reinforced perfluorinated membrane as a function of temperature and humidity. *Electrochem.* **2007**, *75*(2), 197-200.

29. Vilčiauskas, L.; Tuckerman, M. E.; Melchior, J. P.; Bester, G.; Kreuer, K. D. First principles molecular dynamics study of proton dynamics and transport in phosphoric acid/imidazole (2:1) system. *Solid State Ionics* **2013**, *252*, 34-39.

30. Vilčiauskas, L.; Tuckerman, M. E.; Bester, G.; Paddison, S. J.; Kreuer, K.-D. The mechanism of proton conduction in phosphoric acid. *Nat. Chem.* **2012**, *4*(6), 461-466.

31. Iannuzzi, M. Proton transfer in imidazole-based molecular crystals. *J. Chem. Phys.* **2006**, *124*(20), 204710.

32. Iannuzzi, M.; Parrinello, M. Proton transfer in heterocycle crystals. *Phys. Rev. Lett.* **2004**, *93*(2), 025901.

33. Ludueña, G. A.; Kühne, T. D.; Sebastiani, D. Mixed Grotthuss and vehicle transport mechanism in proton conducting polymers from *ab initio* molecular dynamics simulations. *Chem. Mater.* **2011**, *23*(6), 1424-1429.

34. Hayes, R. L.; Paddison, S. J.; Tuckerman, M. E. Proton transport in triflic acid pentahydrate

studied via *ab initio* path integral molecular dynamics. *J. Phys. Chem. A* **2011**, *115*(23), 6112-6124.

35. Yan, L.; Zhu, S. *The theory and practices of molecular dynamic simulations*. Science Press, Beijing, China: 2013: pp 152-156
36. Lin, S. C.; Wu, C. S.; Yeh, J. M.; Liu, Y. L. Reaction mechanism and synergistic anticorrosion property of reactive blends of maleimide-containing benzoxazine and amine-capped aniline trimer. *Polym. Chem.* **2014**, *5*(14), 4235-4244.
37. Marx, D.; Tuckerman, M. E.; Hutter, J.; Parrinello, M. The nature of the hydrated excess proton in water. *Nature* **1999**, *397*(6720), 601-604.
38. Morrone, J. A.; Tuckerman, M. E. *Ab initio* molecular dynamics study of proton mobility in liquid methanol. *J. Chem. Phys.* **2002**, *117*(9), 4403-4413.
39. Morrone, J. A.; Haslinger, K. E.; Tuckerman, M. E. *Ab initio* molecular dynamics simulation of the structure and proton transport dynamics of methanol-water solutions. *J. Phys. Chem. B* **2006**, *110*(8), 3712-3720.
40. Cox, P. J.; Parker, S. F. Maleimide. *Acta Crystallogr. Sect. C* **1996**, *52*, 2578-2580.
41. Jezierska, A.; Panek, J. J.; Koll, A.; Mavri, J. Car-Parrinello simulation of an O–H stretching envelope and potential of mean force of an intramolecular hydrogen bonded system: application to a Mannich base in solid state and in vacuum. *J. Chem. Phys.* **2007**, *126*, 205101.
42. Wierzbicka, E.; Boczar, M.; Wójcik, M. J. Investigation of hydrogen bonds properties in the terephthalic acid crystal, using molecular dynamics method. *Spectrochim. Acta Mol.*

Biomol. Spectrosc. **2014**, *130*, 488-493.

43. Panek, J.; Jezierska, A. Hydrogen bridges of polycyclic aromatic systems with O–H···O bonds—a gas-phase vs. solid-state Car-Parrinello study. *J. Mol. Model.* **2015**, *21*(1), 1-7.
44. Durlak, P.; Mierzwicki, K.; Latajka, Z. Investigations of the very short hydrogen bond in the crystal of nitromalonamide via Car–Parrinello and path integral molecular dynamics. *J. Phys. Chem. B* **2013**, *117*(18), 5430-5440.
45. Goerigk, L.; Grimme, S. A thorough benchmark of density functional methods for general main group thermochemistry, kinetics, and noncovalent interactions. *Phys. Chem. Chem. Phys.* **2011**, *13*(14), 6670-6688.
46. Cohen, A. J.; Mori-Sánchez, P.; Yang, W. Challenges for density functional theory. *Chem. Rev.* **2011**, *112*(1), 289-320.
47. Burke, K. Perspective on density functional theory. *J. Chem. Phys.* **2012**, *136*(15), 150901.
48. Becke, A. D. Correlation energy of an inhomogeneous electron gas: A coordinate-space model. *J. Chem. Phys.* **1988**, *88*(2), 1053-1062.
49. Stare, J.; Panek, J.; Eckert, J.; Grdadolnik, J.; Mavri, J.; Hadzi, D. Proton dynamics in the strong chelate hydrogen bond of crystalline picolinic acid *N*-oxide. A new computational approach and infrared, Raman and INS study. *J. Phys. Chem. A* **2008**, *112*(7), 1576-1586.
50. Troullier, N.; Martins, J. L. Efficient pseudopotentials for plane-wave calculations. *Phys. Rev. B* **1991**, *43*(3), 1993-2006.
51. Lippert, G.; Hutter, J.; Parrinello, M. The Gaussian and augmented-plane-wave density functional method for *ab initio* molecular dynamics simulations. *Theor. Chem. Acc.* **1999**,

103(2), 124-140.

52. Raynaud, C.; Maron, L.; Jolibois, F.; Daudey, J.-P.; Esteves, P. M.; Ramírez-Solís, A. *Ab initio* molecular dynamics: Plane waves vs. local basis: The role of energy cutoff on the convergence of molecular properties. *Chem. Phys. Lett.* **2005**, *414*(1), 161-165.
53. Lin, I.-C.; Coutinho-Neto, M. D.; Felsenheimer, C.; von Lilienfeld, O. A.; Tavernelli, I.; Rothlisberger, U. Library of dispersion-corrected atom-centered potentials for generalized gradient approximation functionals: Elements H, C, N, O, He, Ne, Ar, and Kr. *Phys. Rev. B* **2007**, *75*(20), 205131.
54. Gaigeot, M. P.; Sprik, M. *Ab initio* molecular dynamics computation of the infrared spectrum of aqueous uracil. *J. Phys. Chem. B* **2003**, *107*(38), 10344-10358.
55. Durlak, P.; Latajka, Z. Car-Parrinello and path integral molecular dynamics study of the intramolecular hydrogen bonds in the crystals of benzoylacetone and dideuterobenzoylacetone. *Phys. Chem. Chem. Phys.* **2014**, *16*(42), 23026-23037.
56. Reddy, L. S.; Babu, N. J.; Nangia, A. Carboxamide–pyridine *N*-oxide heterosynthon for crystal engineering and pharmaceutical cocrystals. *Chem. Commun.* **2006**, *13*(1), 1369-1371.
57. Yan, L.; Feng, Q.; Xie, L.; Zhang, D. About the choice of protogenic group for polymer electrolyte membranes: Alkyl or aryl phosphonic acid? *Solid State Ionics* **2011**, *190*(1), 8-17.
58. Sevil, F.; Bozkurt, A. Proton conducting polymer electrolytes on the basis of poly (vinylphosphonic acid) and imidazole. *J. Phys. Chem. Solids* **2004**, *65*(10), 1659-1662.

59. Brunklaus, G.; Schauff, S.; Markova, D.; Klapper, M.; Müllen, K.; Spiess, H.-W. Proton mobilities in phosphonic acid-based proton exchange membranes probed by 1H and 2H solid-state NMR spectroscopy. *J. Phys. Chem. B* **2009**, *113*(19), 6674-6681.

60. Yamada, M.; Honma, I. Anhydrous proton conducting polymer electrolytes based on poly (vinylphosphonic acid)-heterocycle composite material. *Polymer* **2005**, *46*(9), 2986-2992.

61. Bartels, C. Analyzing biased Monte Carlo and molecular dynamics simulations. *Chem. Phys. Lett.* **2000**, *331*(5), 446-454.

62. Vuilleumier, R.; Borgis, D. An extended empirical valence bond model for describing proton transfer in $H^+(H_2O)_n$ clusters and liquid water. *Chem. Phys. Lett.* **1998**, *284*(1), 71-77.

63. Lill, M. A.; Helms, V. Molecular dynamics simulation of proton transport with quantum mechanically derived proton hopping rates (Q-HOP MD). *J. Chem. Phys.* **2001**, *115*(17), 7993-8005.

64. Nagle, J. F.; Tristram-Nagle, S. Hydrogen bonded chain mechanisms for proton conduction and proton pumping. *J. Membr. Biol.* **1983**, *74*(1), 1-14.

65. Lao-ngam, C.; Phonyiem, M.; Chaiwongwattana, S.; Kawazoe, Y.; Sagarik, K. Characteristic NMR spectra of proton transfer in protonated water clusters. *Chem. Phys.* **2013**, *420*, 50-61.

Figure Captions:

Fig. 1 Initial configuration of the CPMD simulated system, notice that the right side image is exactly the same as the left side image but slightly tilted for clarity. Atoms are color coded with grey for C, red for O, blue for N, purple for H, and white for the unbound proton. The unbound proton and two of its closest oxygen atoms are labeled (the labels of the other atoms are irrelevant in this context and thus not showed)

Fig. 2 Energetic evolution in the CPMD simulation, (a) total energy E_{tot}, Kohn-Sham energy E_{KS}, and classic energy $E_{classic}$; (b) kinetic energies of ionic cores K_{ion}, and electrons K_{el}

Fig. 3 Radial distribution functions for the N−O, N−H, and O−H atomic pairs

Fig. 4 (a) Bond stretching vibrational spectra of MI evaluated via FFT of the time-dependences of interatomic distances from CPMD simulation, (b) experimental FTIR

Fig. 5 (a) Velocity autocorrelation functions and (b) their corresponding spectra

Fig. 6 (a) Probability distributions of interatomic distances of O39–O48, H1–O39, and H1–O48; (b,c) overall probability distributions of interatomic distances of H1–O39 and H1–O48 given the interatomic distance of O39–O48, notice that the crossover points of proton hopping are indicated by the "X" signs; (d) the potential energy surfaces along the reaction coordinate that define the proton exchange between two MI molecules in an isolated system consisting of only two MI molecules and an extra proton. CPMD simulations are carried in NVT ensemble at 363.15 K, and DFT calculations are evaluated at theory level of ωB97X-D/6-311+G(2d,p)

Fig. 7 Arrhenius plot for the proton hopping frequency in solid state MI system

Supplementary Information:

Table S1 Atomic coordinates of the initial configuration (unit: Å)

Table S2 Energetic fluctuations during the CPMD simulation in NVT ensemble at five different temperatures (the corresponding standard deviations are shown in brackets)

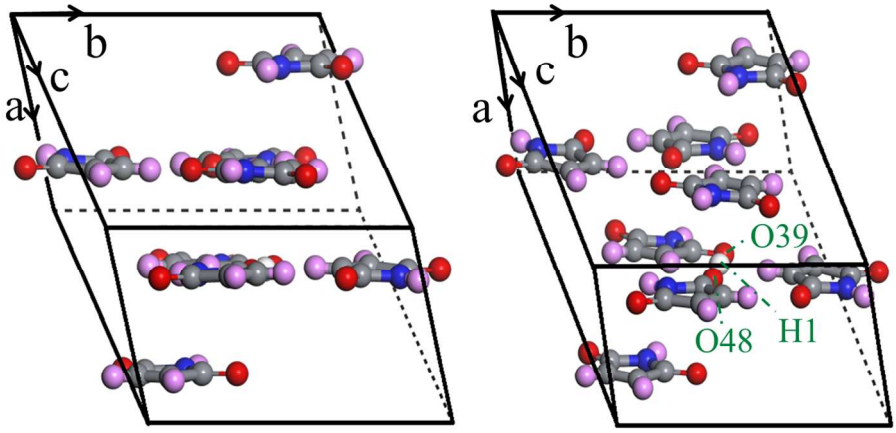

Fig. 1 Initial configuration of the CPMD simulated system, notice that the right side image is exactly the same as the left side image but slightly tilted for clarity. Atoms are color coded with grey for C, red for O, blue for N, purple for H, and white for the unbound proton. The unbound proton and two of its closest oxygen atoms are labeled (the labels of the other atoms are irrelevant in this context and thus not showed)
266x136mm (150 x 150 DPI)

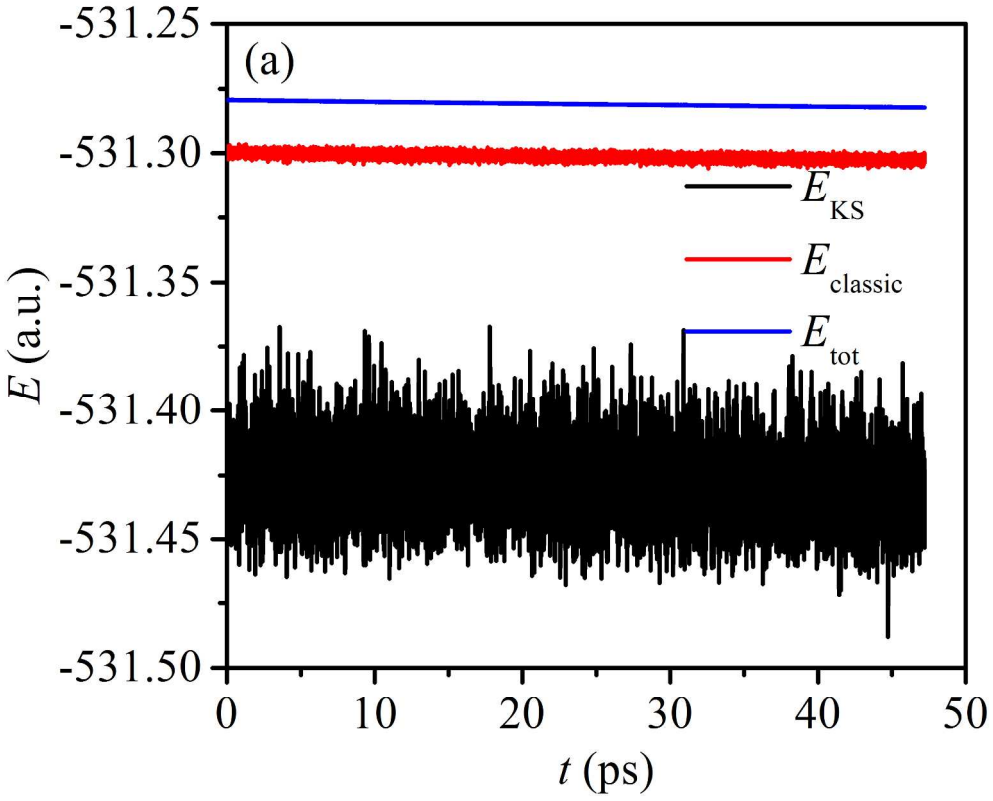

Fig. 2 Energetic evolution in the CPMD simulation, (a) total energy Etot, Kohn-Sham energy EKS, and classic energy Eclassic; (b) kinetic energies of ionic cores Kion, and electrons Kel
254x203mm (300 x 300 DPI)

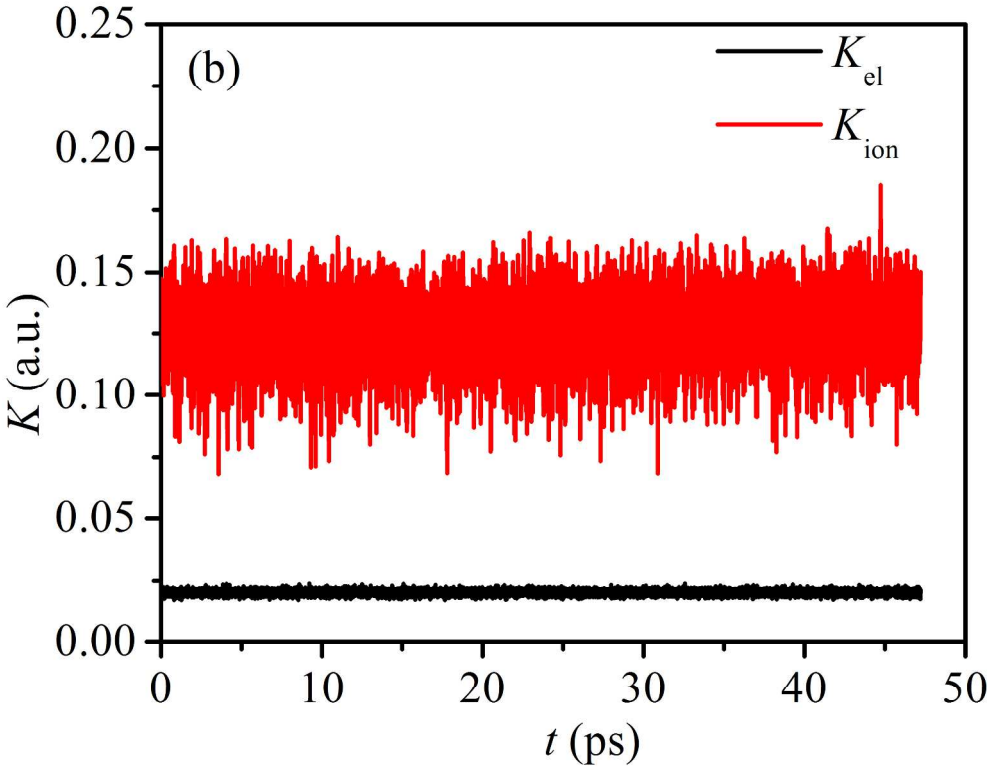

Fig. 2 Energetic evolution in the CPMD simulation, (a) total energy Etot, Kohn-Sham energy EKS, and classic energy Eclassic; (b) kinetic energies of ionic cores Kion, and electrons Kel
254x203mm (300 x 300 DPI)

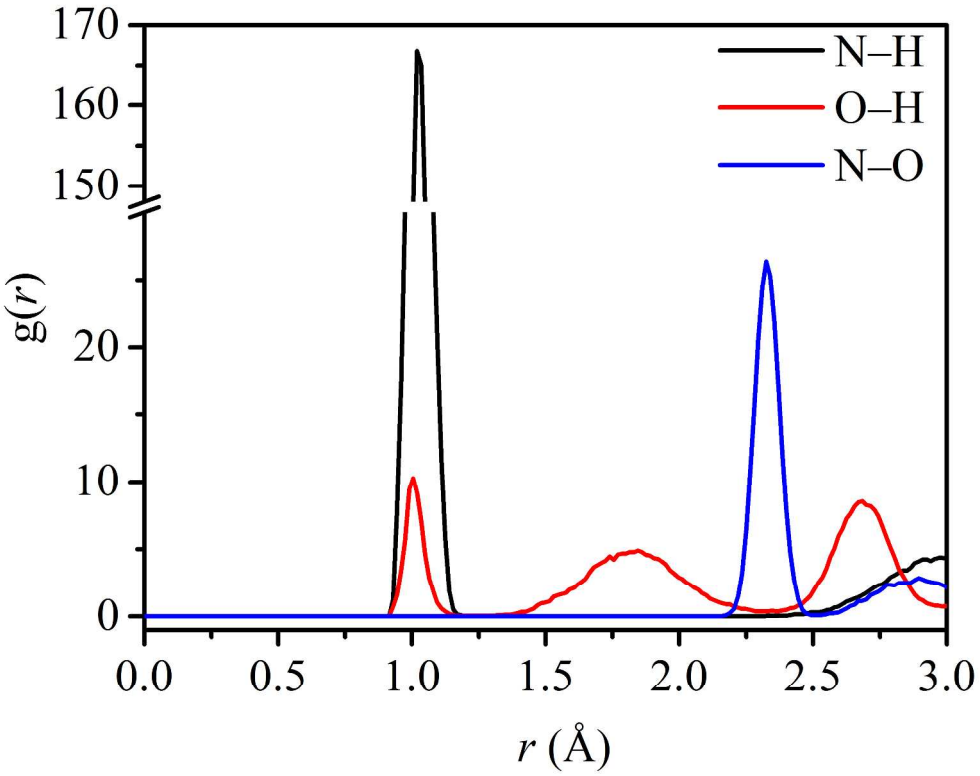

Fig. 3 Radial distribution functions for the N–O, N–H, and O–H atomic pairs
304x243mm (300 x 300 DPI)

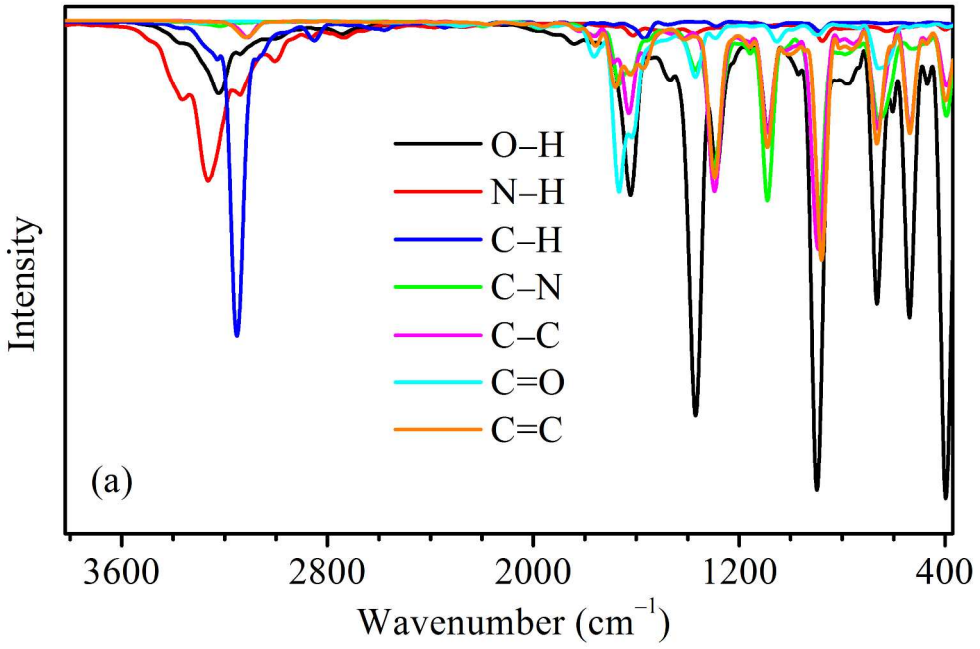

Fig. 4 (a) Bond stretching vibrational spectra of MI evaluated via FFT of the time-dependences of interatomic distances from CPMD simulation, (b) experimental FTIR
254x169mm (300 x 300 DPI)

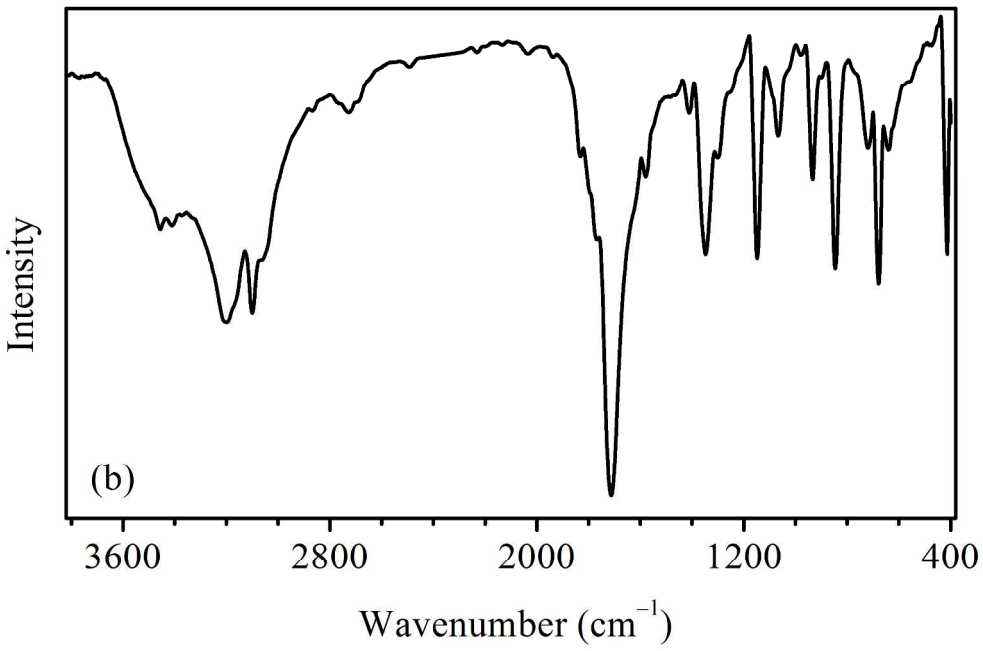

Fig. 4 (a) Bond stretching vibrational spectra of MI evaluated via FFT of the time-dependences of interatomic distances from CPMD simulation, (b) experimental FTIR
254x169mm (300 x 300 DPI)

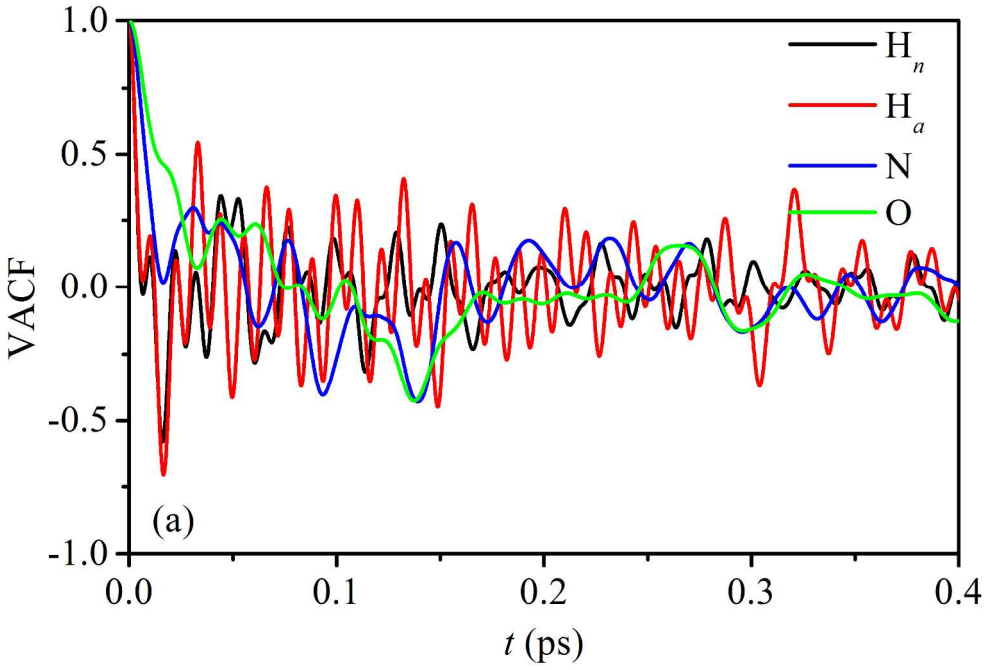

Fig. 5 (a) Velocity autocorrelation functions and (b) their corresponding spectra
254x169mm (300 x 300 DPI)

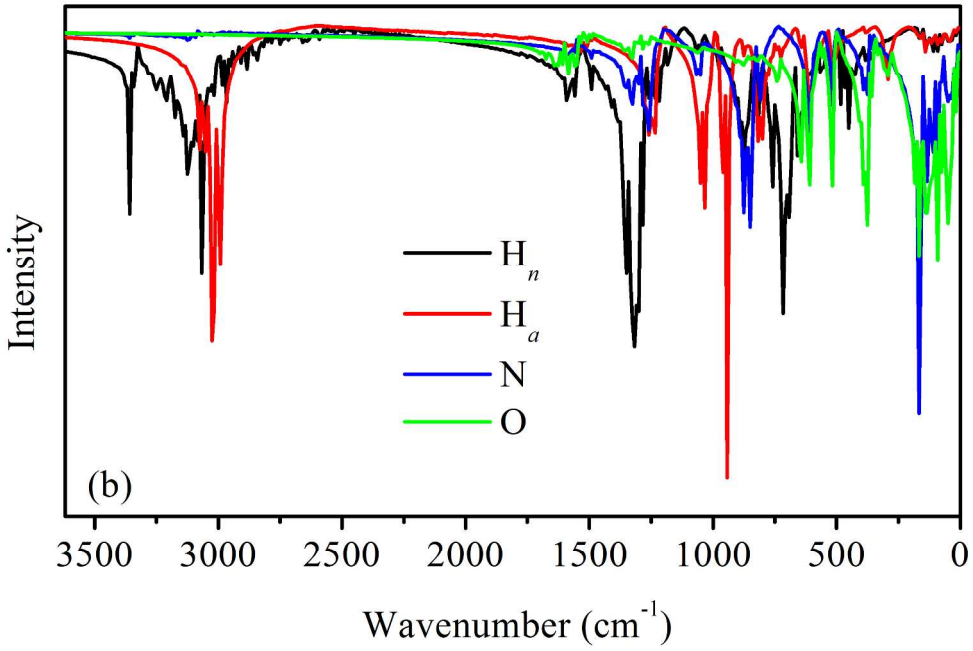

Fig. 5 (a) Velocity autocorrelation functions and (b) their corresponding spectra
254x169mm (300 x 300 DPI)

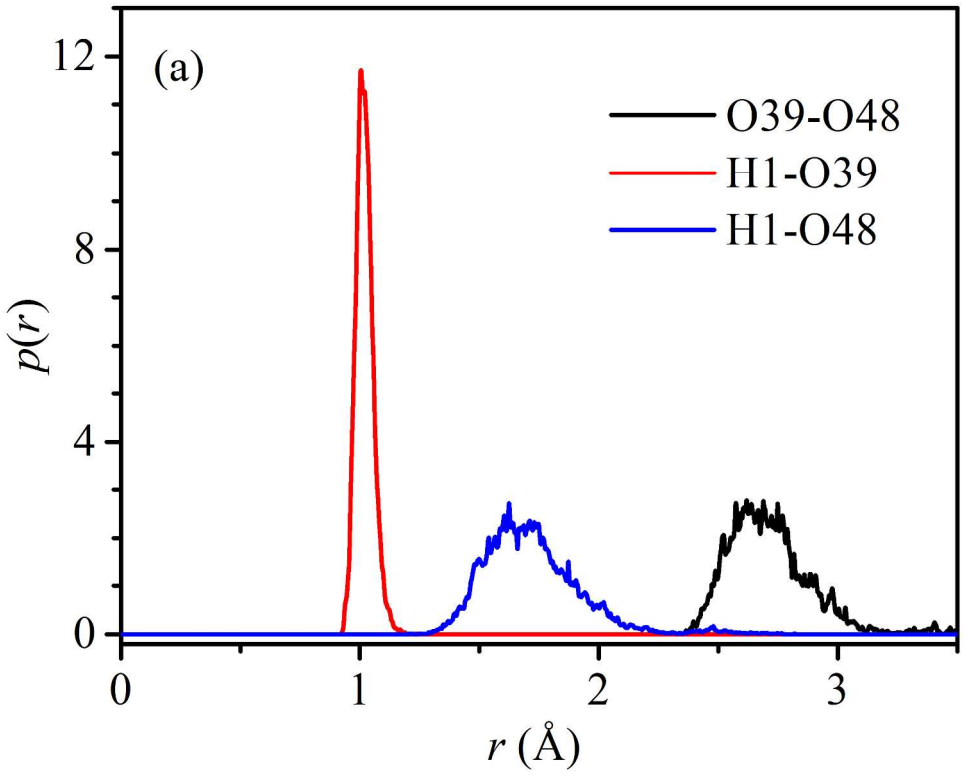

Fig. 6 (a) Probability distributions of interatomic distances of O39–O48, H1–O39, and H1–O48; (b,c) overall probability distributions of interatomic distances of H1–O39 and H1–O48 given the interatomic distance of O39–O48, notice that the crossover points of proton hopping are indicated by the "X" signs; (d) the potential energy surfaces along the reaction coordinate that define the proton exchange between two MI molecules in an isolated system consisting of only two MI molecules and an extra proton. CPMD simulations are carried in NVT ensemble at 363.15 K, and DFT calculations are evaluated at theory level of ωB97X-D/6-311+G(2d,p).
254x203mm (300 x 300 DPI)

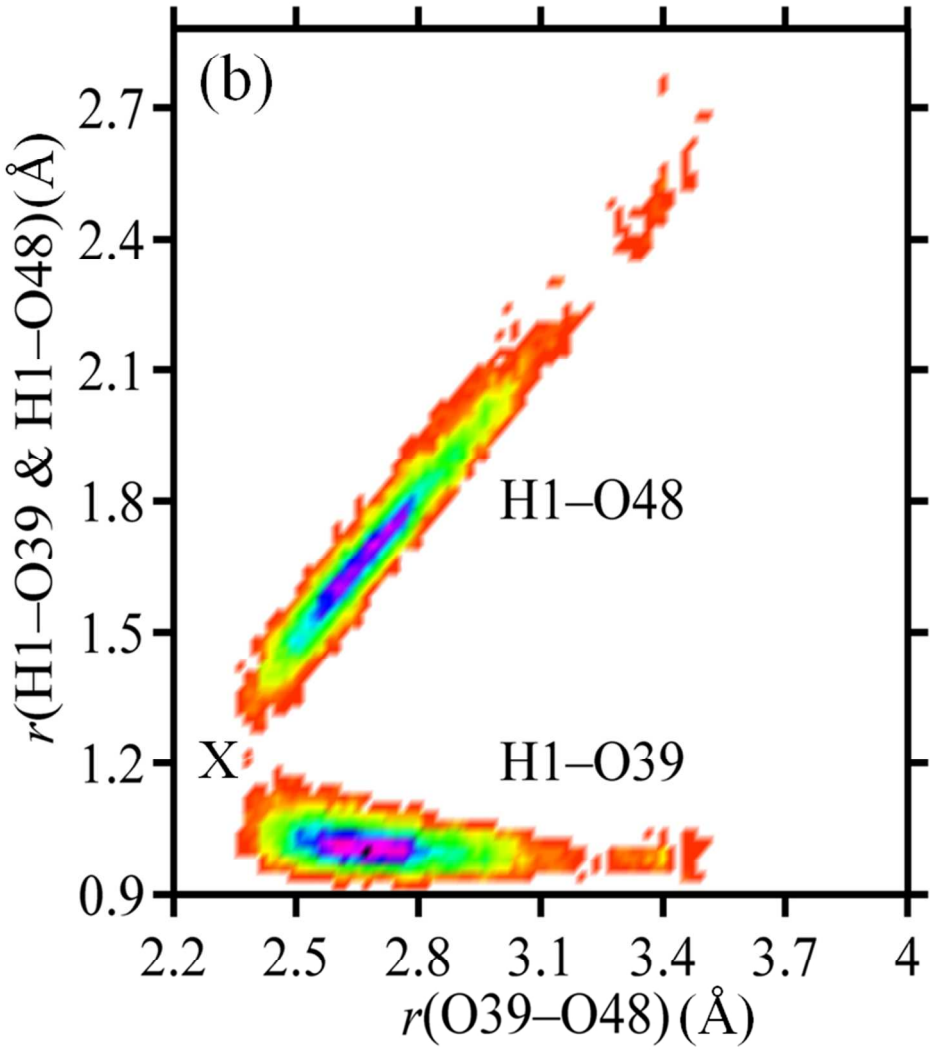

Fig. 6 (a) Probability distributions of interatomic distances of O39–O48, H1–O39, and H1–O48; (b,c) overall probability distributions of interatomic distances of H1–O39 and H1–O48 given the interatomic distance of O39–O48, notice that the crossover points of proton hopping are indicated by the "X" signs; (d) the potential energy surfaces along the reaction coordinate that define the proton exchange between two MI molecules in an isolated system consisting of only two MI molecules and an extra proton. CPMD simulations are carried in NVT ensemble at 363.15 K, and DFT calculations are evaluated at theory level of ωB97X-D/6-311+G(2d,p)
140x154mm (300 x 300 DPI)

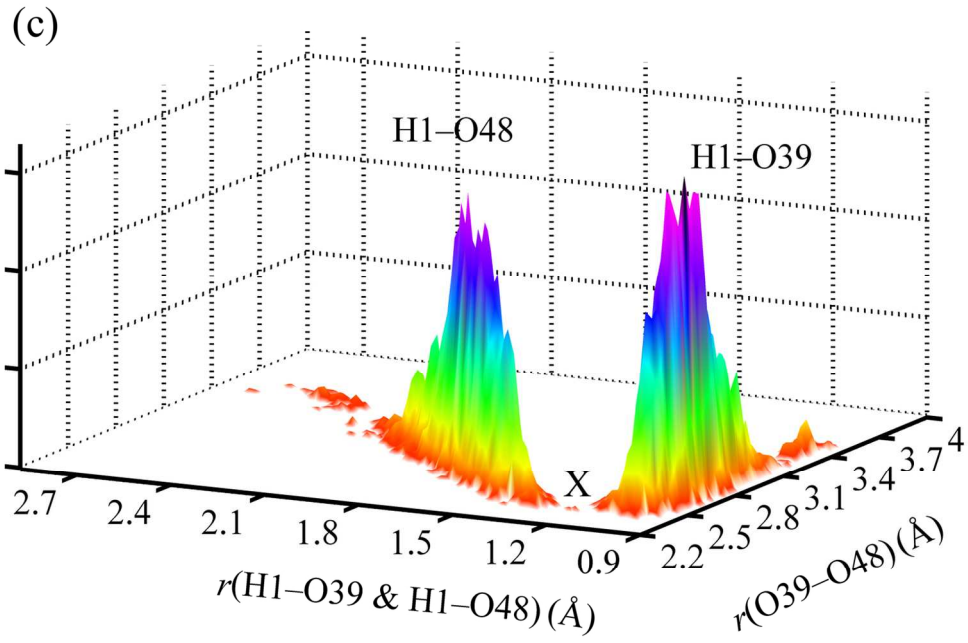

Fig. 6 (a) Probability distributions of interatomic distances of O39–O48, H1–O39, and H1–O48; (b,c) overall probability distributions of interatomic distances of H1–O39 and H1–O48 given the interatomic distance of O39–O48, notice that the crossover points of proton hopping are indicated by the "X" signs; (d) the potential energy surfaces along the reaction coordinate that define the proton exchange between two MI molecules in an isolated system consisting of only two MI molecules and an extra proton. CPMD simulations are carried in NVT ensemble at 363.15 K, and DFT calculations are evaluated at theory level of ωB97X-D/6-311+G(2d,p).
135x91mm (300 x 300 DPI)

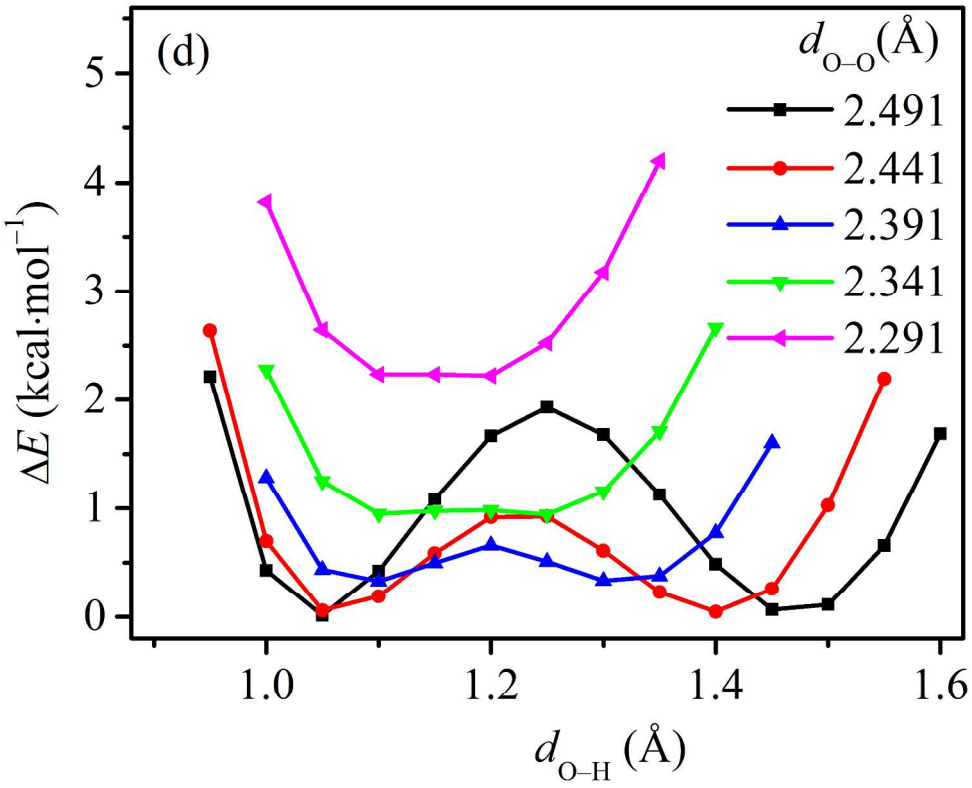

Fig. 6 (a) Probability distributions of interatomic distances of O39–O48, H1–O39, and H1–O48; (b,c) overall probability distributions of interatomic distances of H1–O39 and H1–O48 given the interatomic distance of O39–O48, notice that the crossover points of proton hopping are indicated by the "X" signs; (d) the potential energy surfaces along the reaction coordinate that define the proton exchange between two MI molecules in an isolated system consisting of only two MI molecules and an extra proton. CPMD simulations are carried in NVT ensemble at 363.15 K, and DFT calculations are evaluated at theory level of ωB97X-D/6-311+G(2d,p).
254x203mm (300 x 300 DPI)

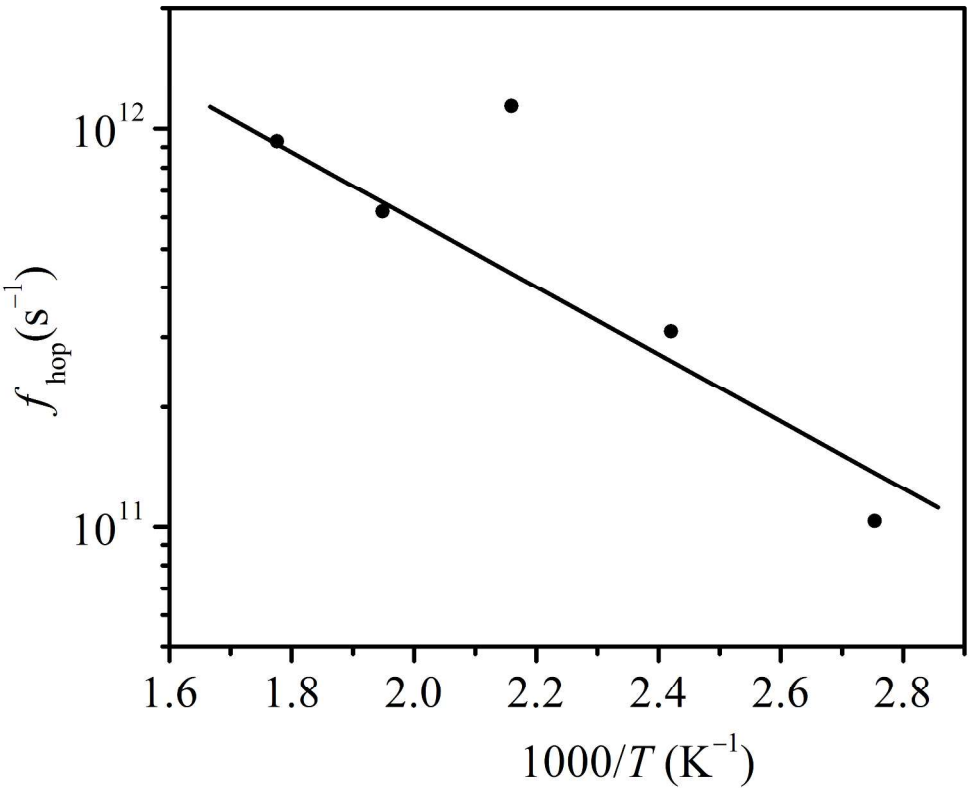

Fig. 7 Arrhenius plot for the proton hopping frequency in solid state MI system
254x203mm (300 x 300 DPI)